Eur. Phys. J. D **30**, 235–241 (2004)
DOI: 10.1140/epjd/e2004-00084-4

THE EUROPEAN PHYSICAL JOURNAL D

# Soft X-ray contact microscopy of nematode Caenorhabditis elegans*

G. Poletti[1,a], F. Orsini[1], D. Batani[2], A. Bernardinello[2], T. Desai[2], J. Ullschmied[3], J. Skala[3], B. Kralikova[3], E. Krousky[3], L. Juha[3], M. Pfeifer[3], Ch. Kadlec[3], T. Mocek[3], A. Präg[3], O. Renner[3], F. Cotelli[4], C. Lora Lamia[4], and A. Zullini[5]

[1] INFM, CIMAINA, and Istituto di Fisiologia Generale e Chimica Biologica, Università di Milano, Via Trentacoste 2, 20134 Milano, Italy
[2] Dipartimento di Fisica "G.Occhialini", Università di Milano Bicocca, Piazza della Scienza 3, 20126 Milano, Italy
[3] PALS Research Centre, Za Slovankou 3, 18221 Prague 8, Czech Republic
[4] Dipartimento di Biologia, Università di Milano, Via Celoria 26, 20133 Milano, Italy
[5] Dipartimento di Biotecnologie e Bioscienze, Università di Milano Bicocca, Piazza della Scienza 2, 20126 Milano, Italy

Received 18 February 2004
Published online 29 June 2004 

**Abstract.** Soft X-ray Contact Microscopy (SXCM) of *Caenorhabditis elegans* nematodes with typical length ∼800 $\mu$m and diameter ∼30 $\mu$m has been performed using the PALS laser source of wavelength $\lambda = 1.314$ $\mu$m and pulse duration $\tau$(FWHM) = 400 ps. Pulsed soft X-rays were generated using molybdenum and gold targets with laser intensities $I \geq 10^{14}$ W/cm$^2$. Images have been recorded on PMMA photo resists and analyzed using an atomic force microscope operating in contact mode. Cuticle features and several internal organs have been identified in the SXCM images including lateral field, cuticle annuli, pharynx, and hypodermal and neuronal cell nuclei.

**PACS.** 42.62.Be Biological and medical applications – 07.85.Tt X-ray microscopes – 87.59.Bh X-ray radiography

## 1 Introduction

An intense laser beam focused on a solid target produces a micro-size hot, dense plasma over duration comparable to the laser pulse. Such plasmas are versatile laboratory devices; in particular they are used as high brightness soft X-ray sources, whose spectrum can be adjusted by changing the target material and laser beam parameters [1–3]. One of the important applications of soft X-rays from such source is Soft X-ray Contact Microscopy (SXCM) of living biological specimens.

This technique permits to image the biological organisms in their living environment by using soft X-ray photons in the water window range (wavelength 2.34−4.42 nm, i.e. between the absorption edges of carbon and oxygen). When these irradiate a biological sample, a natural contrast between the cytoplasm (mainly water) and other structures of the cell (cellular wall, nucleus and other organelles) is obtained. The cytoplasm remains transparent to the incident radiation whereas the other structures of the cells (mostly carbon) become opaque. Thus, the existence of the water window permits to get high contrast images of organic materials directly in a liquid environment [4,5]. Hence X-ray microscopy allows obtaining images of living biological samples against the dehydrated (dead) samples obtained by other high-resolution microscopy techniques (living samples are routinely imaged in optical microscopy but resolution is limited by wavelength to a fraction of a micron).

In SXCM, a 1:1 image (no magnification) is obtained by placing the biological sample directly in contact with a sensitive element (here a PMMA photo resist). The recorded image can then be analyzed with an atomic force microscope (AFM). The exposure time is very brief, of the order of the laser pulse, i.e. far below the time for the biological deterioration of the samples [6,7]. Thus, even if the X-ray dose is high and may kill the cells, nevertheless, they are imaged when still alive.

X-rays in the water window range can be produced using low and high $Z$ materials as targets. There are certain advantages of using a high $Z$ target for producing X-rays as X-ray conversion efficiency is high and copious soft X-rays are generated due to bremsstrahlung and recombination processes. However, there is a large spill-over of radiation around the water window in the case of high $Z$ materials. Images can still be obtained even in this case, but contrast is due to a different local density in the sample rather than to different absorption between water and the biological material, and it is then usually reduced.

* A color version of the figures is available in electronic form at `http://www.edpscience.org`.

[a] e-mail: `Giulio.Poletti@unimi.it`

In this paper, we report the analysis of SXCM images of *Caenorhabditis elegans* (*C. elegans*) biological samples. X-ray spectra were also recorded with X-ray spectrometers, and used to obtain the corresponding plasma parameters, plasma density and temperature by spectroscopic analysis. Images obtained on the PMMA photo resists were analyzed using AFM operating in contact mode. SXCM has already been used to image biological samples such as yeast cells, unicellular green algae, human red blood cells [8–11]. The goal of the present paper was to explore the potentialities of the technique to study complex, multi-cellular organisms. To this aim, the well biological characterized *C. elegans* nematode has been chosen. It is the first time that small (semi-microscopic) but complex, multi-cellular samples are studied by SXCM.

## 2 Experiments

Experiments were performed using the PALS Asterix Iodine laser system in Prague [12], which emits 1.314 $\mu$m radiation in fundamental. Laser pulse duration was $\sim$400 ps. The maximum optical energy in a single beam was 600 J and the beam diameter at the entrance of the plasma chamber was $\sim$290 mm. Laser radiation was focused on the target surface using a $f = 600$ mm focusing lens and the intensity was varied in the range $\sim 10^{14}-10^{16}$ W/cm$^2$ by either changing the laser spot area (focal spot was varied from 150 to 600 $\mu$m) or changing the incident laser energy. The interaction chamber was evacuated to better than $10^{-4}$ mbars.

### 2.1 X-ray spectroscopy

Three types of planar solid targets were used viz. Teflon ($CF_2$), molybdenum (Mo) and gold (Au) to produce X-rays. Biological samples were irradiated with X-rays produced from high $Z$ materials. Gold and molybdenum have similar flux in water window regime [13]. A flat crystal Bragg's spectrometer was used to record the spectrum emitted by the plasma. X-ray spectra can provide information on the properties of the plasma, in particular plasma density and temperature during the process of X-ray emission, by the analysis of the spectral shape, spectral width, position of different lines and their relative intensities [14]. Teflon targets have a particularly simple K-shell centred at 0.9 keV and are particularly useful for such a diagnostic purpose.

The spectrometer used in the experiment had a RbAp crystal ($2d = 2.6121$ nm). Time and space integrated X-ray spectra were recorded on Kodak DEF films. In the present experiment due to the presence of biological sample holders, the spectrometer was located at a distance of 6.5 cm from the X-ray source at an angle of 75° to the laser axis. Spectra were recorded for every exposure of the biological sample putting a 100 $\mu$m slit on the spectrometer. An aluminium foil of 5 $\mu$m acted as a filter for Teflon target, whereas a 14 $\mu$m aluminium foil was used for gold and molybdenum targets.

X-rays are produced from the plasma over a time span ($\tau_x$) comparable to laser pulse duration ($\tau$). Actually X-ray emission has been largely investigated as a tool for plasma diagnostics. In the case of molybdenum target, soft X-rays are due to N shell whereas for gold targets from N and O shells.

### 2.2 Description of the biological specimen and exposure to X-rays

The roundworm *C. elegans* is a small, free-living soil nematode found commonly in many part of the world. *C. elegans* has two sexes, a self-fertilizing hermaphrodite and a male, with both sexes having a similar general anatomy. The two adult sexes are each about 1 mm in length and 40 $\mu$m in diameter; the hermaphrodite has only 959 somatic cells, the adult male 1031, plus a variable number of germ cells (up to about 2000). *C. elegans* is a rapidly growing organism, develops through four juveniles stages (J1−J4) separated by moults in which the old cuticle is shed and replaced by a new one formed underneath. The life cycle takes about three days in optimum conditions. The natural environment of *C. elegans* is the soil where the organism mainly feeds on bacteria, but it can be easily raised in the laboratory (a 9 cm diameter plate can support the growth of 100 000 animals). The simple body plan, convenience of manipulation, and short life cycle of *C. elegans* make it one of the most widely used model system to study a variety of problems in animal biology (aging, molecular biology, genetics).

These samples are much larger than unicellular samples and provide the opportunity to explore the capability of SXCM technique as a suitable tool to image complex organisms. Also, these samples are strong and can survive for more than 30 minutes under stress conditions. This allowed preparation of several samples before their exposure to X-radiation.

Because of its several notable features and its relatively simple characteristics we selected *C. elegans* as model for our experiments.

The first step in the experiment was to put the samples in the sample holders. A droplet of water containing the biological specimens was sandwiched between a silicon nitride window and a photo resist (PMMA-Polymethilmetacrylate) with the minimum possible level of water (actually, close to the maximum specimen diameter). The assembly of the specimen holder was similar to that of earlier works [11]. X-rays were incident on the silicon nitride window, which is transparent to visible and X-radiation. Usually 4−5 samples were simultaneously exposed to every laser shot. The sample holders were placed at two different distances (5 and 10 cm from the X-ray source) at an angle of 45° to the laser axis.

The photo resist was a PMMA square with a 250 $\mu$m size. Passing through the sample X-rays are absorbed in a different way from the various parts of the specimen and therefore different parts of the photo resist receive different X-rays doses, according to the sample characteristics. The PMMA is a polymer whose chain

structure may be broken by soft X-rays, so that irradiation reduces the polymer size and makes it more soluble to chemical development. Then the chemical development of the photo resist gives rise to a profile of the sample, whose height depends on the absorbed X-rays dose. The exposed PMMA photo resist was developed at room temperature with a 1:1 mixture of isopropyl alcohol and methylisobutylketone for a fixed time of 30 seconds before being cleaned and washed with isopropyl alcohol. The specimen possibly left on the photo resist was removed by a sodium hypochlorite solution before chemical development. In our experiment, the height of the whole profile was ≈400 nm while the traces of the internal organs were superimposed on this layer and of the order of a few nanometres only. This profile is analysed with the AFM.

### 2.3 AFM instrumentation

After chemical development, the photo resists were analyzed using an AutoProbe CP Research AFM (ThermoMicroscopes, Sunnyvale, CA, USA). In AFM topography images the higher zones correspond to areas of the sample where the density of carbon was higher giving rise to a higher X-ray absorption. AFM measurements were made in air in contact mode (constant force mode) collecting simultaneously the topography images and the associated error signal images.

AFM probes the surface of a sample with a sharp tip located at the free end of a cantilever. The forces between the tip and the sample surface cause the cantilever to bend or deflect. The measured cantilever deflection as the tip is scanned over the sample allows to generate a map of surface topography. In contact mode, the AFM tip makes a soft "physical contact" with the sample surface. As the scanner gently traces the tip across the sample, the contact force causes the cantilever to bend to accommodate changes in topography. Once the AFM detects deflection, the spatial variations of the cantilever deflection can be directly used to generate the topographic data set (constant height mode). Alternatively (constant force mode), it can be used as input to a feedback circuit that moves the scanner up and down in $z$-direction responding to the topography by keeping the cantilever deflection constant. In this case the image is generated from the scanner motion. In constant force mode the speed of scanning is limited by the response time of the feedback circuit, but the total force exerted on the sample by the tip is well controlled so that this mode is generally preferred for most applications.

In the error signal images, the feedback loop serves as a high-pass filter that filters out the low spatial frequency components leaving only the high spatial frequency components of the sample surface to be displayed. In this way, error signal images are generated which, although do not give quantitative information of surface topography, provide results, which are very useful in giving a direct imaging of the sample surface and easier to be interpreted by visual inspection.

Microfabricated V-shaped silicon cantilevers with silicon conical tip (ThermoMicroscopes, Sunnyvale, CA, USA) of resonant frequency of approximately 45 kHz and a force constant of 0.4 N/m were used. AFM images were processed using the Image Processing Data Analysis 2.0 software provided by ThermoMicroscopes.

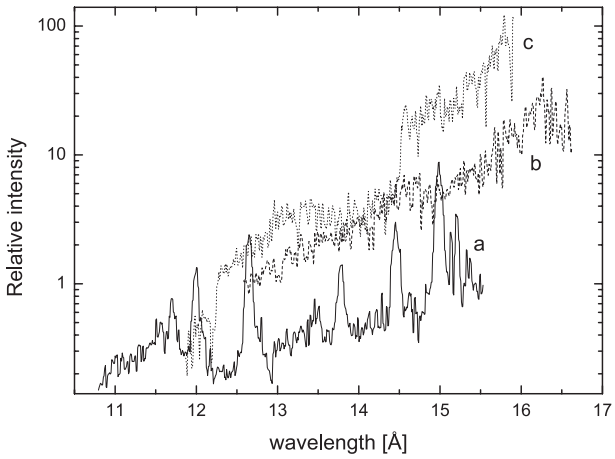


**Fig. 1.** X-ray intensity versus X-ray wavelength for (a) Teflon, (b) gold and (c) molybdenum. Laser intensity on the target surface was $5\times10^{14}$, $2.6\times10^{14}$, $2.75\times10^{14}$ W/cm$^2$ respectively. Al filter thickness was 5 $\mu$m for Teflon and 14 $\mu$m for Au and Mo.

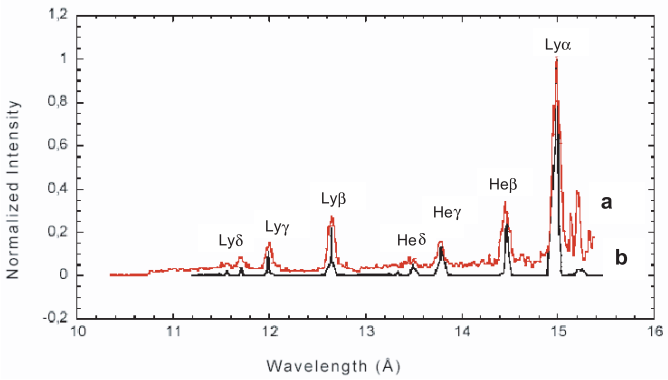


**Fig. 2.** Normalized X-ray intensity versus X-ray wavelength for Teflon target: (a) experimental results, (b) calculated by RATION.

## 3 Results and discussion

### 3.1 X-ray emission spectra

X-ray spectra recorded at laser intensity $I \sim 10^{14}$ W/cm$^2$ on target from Teflon, gold and molybdenum plasmas are shown in Figures 1a, 1b and 1c respectively. X-ray intensities were corrected by taking into account the X-ray film response [15], crystal reflectivity [16] and filter transmission [17]. The dominant bound-bound transitions are marked for Teflon plasma in Figure 2. Prominent and separated satellite lines were observed at lower photon energy ($\lambda > 15$ Å) for Teflon.

The continuum spectrum emitted by gold targets (Fig. 1b) shows an exponential decrease with increasing photon energy. The electron temperature estimated from

the slope of the continuum equals to $T_e = 90 \pm 10$ eV. The analogous evaluation of the continuum emitted by the molybdenum plasma (Fig. 1c) gives a temperature $T_e = 120 \pm 10$ eV.

### 3.2 Analysis of the X-ray emission spectra

Figure 2a shows the X-ray intensity versus X-ray wavelength from Teflon plasma. Spectra clearly shows the H-like and He-like groups of lines and strong satellite lines. From these lines we can estimate the plasma density and temperature.

Laser produced plasmas are inhomogeneous: X-rays are generated from different plasma regions with different densities and temperatures, as the plasma expands from the target surface. Therefore a single temperature and density may not be appropriate to characterize such plasmas. However, we tried to interpolate experimental spectra using the minimum number of parameters i.e. a single density and a single temperature which must be then considered as a space and time average of the evolving plasma parameters during the process of X-ray emission. Line radiation and continuum are emitted due to different mechanism in the plasma. Line radiation is emitted due to electron transitions between bound states of an ion; the spectrum of the emitted radiation therefore consists of lines at distinct wavelengths. Instead the free-free and free bound electron transitions give rise to a continuum. In the present case, carbon emission lines (K-shell) were not recorded being below the detectable range of the RbAP crystal. However, the presence of carbon (33% in Teflon) implies the existence of lines and recombination radiation due to carbon plasma. This can be seen as a continuum superimposed on fluorine ion lines. The continuum appearing at higher energy is mainly due to fluorine ions. The exponential interpolation of the continuum at high photon energy from Teflon spectra shows an average plasma temperature $T_e = 125 \pm 5$ eV.

We also used the code RATION to simulate X-ray spectra. This code was developed by Lee at LLNL laboratory [18] and used to generate K shell spectra from carbon ($Z = 6$) to iron ($Z = 26$). Experimentally recorded Teflon spectra correspond to the X-ray wavelength in the range $10-16$ Å. The calculations assumed fluorine ions ($Z = 9$) with 33% impurity from carbon, spot size of the order of laser focal spot on the target surface (150 $\mu$m) and instrumental width (FWHM) of 2 eV. Plasma was considered to be in Non Local Thermodynamic Equilibrium (NLTE). Figure 2 shows the experimental spectra (a) and the simulated spectra (b). The agreement is sufficiently good using plasma temperature and density respectively equal to $T_e = 145$ eV and $N_e = 4.8 \times 10^{20}$ cm$^{-3}$. However, the structures of the satellite lines are not well reproduced.

### 3.3 Biological images

Before discussing the results it is important to point out that this is a preliminary experiment aimed at testing the possibility of using SXCM with complex semi-microscopic organisms. For this reason, we choose a well-known biological sample, such as *C. elegans*, which it is often used as a laboratory model in biology and, hence, it is well-known. This allows the identification of the structures observed in SXCM by comparison with the results obtained with other techniques, already present in the scientific literature. Of course, this implies that it is unlikely to observe new structures, or to discover new features, but, again, we emphasize that this was *not* the goal of the present experiment.

Several problems have been encountered which must be addressed in order to guarantee better results in the future.

First of all, only about 15% of the exposed photo resists (approximately 60) gave good images. Apart from the breakage of several extremely delicate silicon nitride windows during the various phases of the experiment, the probability of having a single *C. elegans* on the PMMA windows was low. In many cases, we either had no biological samples in the $250 \times 250$ $\mu$m$^2$ window, or on the contrary particularly *crowded* photo resists made the analysis of a single worm very difficult.

Second, *C. elegans* of different sizes and therefore in different development phases were used in order to have a wide spectrum of specimens having different overall dimensions (length ranging from 250 to 1000 $\mu$m and corresponding diameters ranging from 10 to 30 $\mu$m) and slightly different characteristics that could give information on the performances of the technique. As a consequence, the thickness of water around the various specimens was not constant. Indeed during sample preparation, we try to make it as thin as possible, which means that it will be of the order of diameter of the largest specimen present on the photo resist. This may have influenced the quality of several images.

Third, in accordance with the experience gained in previous experiments performed on yeast cells [11], preset development times (30 seconds) were used. Due to the completely different biological samples it is possible that different development times could have given more detailed or precise information (the effect of changing the development times will be studied in future experiments).

Despite these problems, good results were nevertheless obtained from *C. elegans* of different size; this confirms that the technique can be used as a research tool for a quite large range of specimen size. Indeed, the recorded images are significant and quite well related to the existing biological knowledge, both qualitatively and quantitatively.

A schematic scale line drawing of a *C. elegans* nematode has been reported in Figure 3 in order to show the major anatomical features and help the identification of the structures imaged by SXCM.

Figure 4 shows as reconstruction of a SXCM imprint on a PMMA photo resist of a *C. elegans* nematode, obtained combining 72 error signal AFM images. The scan area of the single AFM image was of $20 \times 20$ $\mu$m$^2$. Error signal and not topography AFM images have been used because,

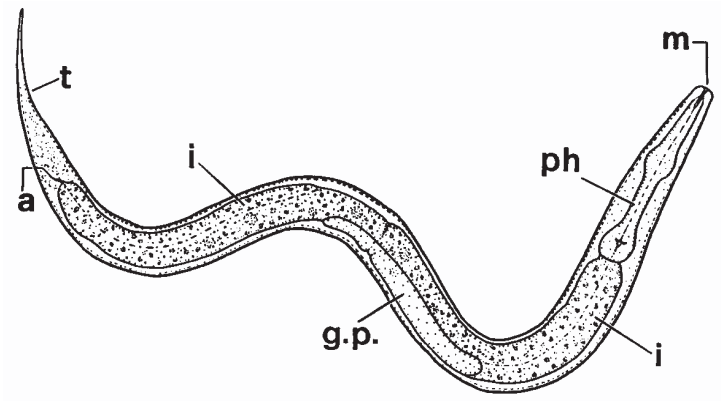


**Fig. 3.** Schematic scale line drawing of the major anatomical features of *Caenorhabditis elegans* nematode: (a) anus; (g.p.) genital primordium; (i) intestine; (m) mouth; (ph) pharynx; (t) tail.

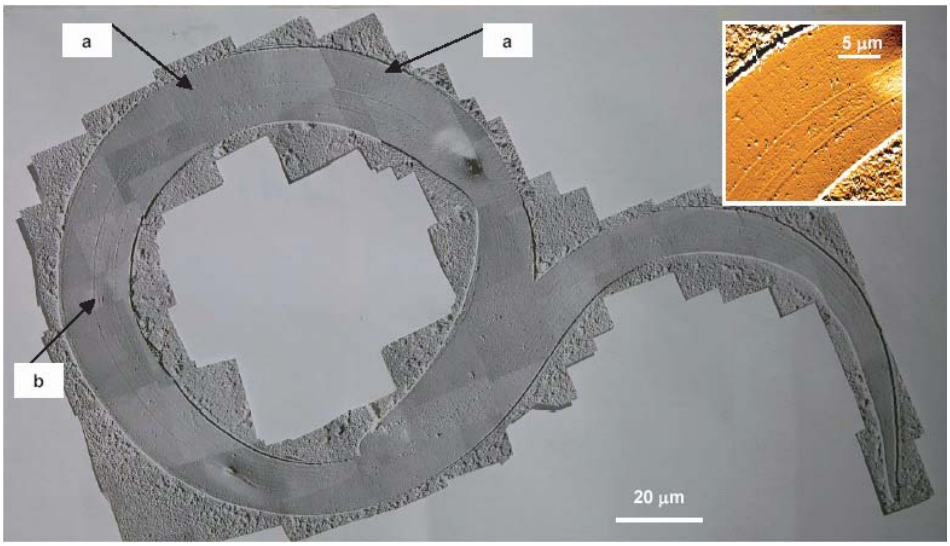


**Fig. 4.** Reconstruction of a SXCM imprint of a *Caenorhabditis elegans* nematode on a PMMA photo resist, obtained combining 72 error signal AFM images. Each single AFM image has a scan area of 20 × 20 $\mu$m$^2$. The nematode length is 500 $\mu$m approximately. Cuticle annuli (a) are visible in regular transverse rows perpendicular to the tri-ridged lateral field (b). In the insert a single error signal AFM image is showed. The cuticle is circumferentially indented at regular 1.1 $\mu$m intervals, creating pleated-appearing annuli.

as quoted above, error signal images allow to better highlight fine structural features of the surface. The sample length is 500 $\mu$m approximately. The figure clearly shows both the transversal annuli and the tri-ridged lateral field (*alae*), which run longitudinally on the lateral surfaces of the cuticle, along the whole length of the body. A single error signal image (see insert), chosen among those used in Figure 4, allows to see the cuticle annuli more easily. AFM images allowed to measure cuticle structural details with nanometre precision. In particular, the single cuticle annulus shows a width of about 1.1 $\mu$m while a constant distance of 220 nm has been found between two consecutive annuli. The single lateral ala shows a width of about 330 nm while a distance of 770 nm has been observed between two consecutive alae. These results are in good agreement with data reported in literature [19]. However it is worth to remark that, while our images clearly show the alae characteristic features, according to Cox et al., longitudinal ridges are not observed on lateral surface of the cuticle of the juvenile stage (500 $\mu$m long).

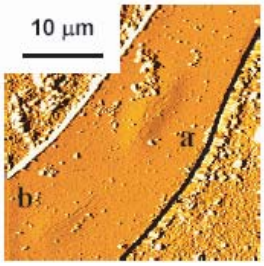


**Fig. 5.** 30 × 30 $\mu$m$^2$ error signal AFM image of a SXCM imprint on a PMMA photo resist of a *Caenorhabditis elegans* nematode. The pharyngeal metacorpus (a) and terminal bulb (b) are clearly visible.

Besides cuticle features, several microscopic images of internal parts of the nematode have been obtained. Figure 5 reports a 30 × 30 $\mu$m$^2$ error signal AFM image of a SXCM imprint representing the anterior of the animal and showing two distinct oval structures. These have

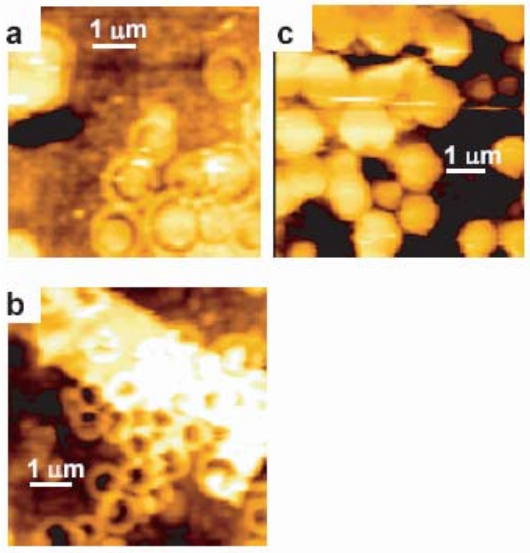


**Fig. 6.** $6 \times 6$ $\mu$m$^2$ topography AFM images of a SXCM imprint on a PMMA photo resist of a *Caenorhabditis elegans* nematode. The images have been collected in the central region of nematode. Nuclei of three different cell types have been individuated: (a) hypodermal and gut nuclei, round with a large, prominent nucleolus, having the characteristic "fried egg" appearance; (b) neuronal nuclei, smaller, round and without prominent nucleoli; (c) other type of nuclei.

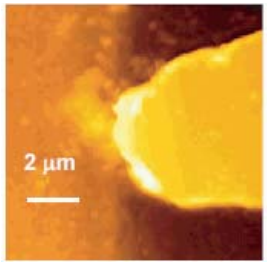


**Fig. 7.** $10 \times 10$ $\mu$m$^2$ topography AFM image of a SXCM imprint on a PMMA photo resist of a *Caenorhabditis elegans* nematode. Profile of the nematode anterior body end.

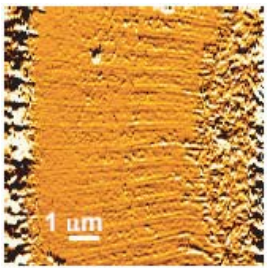


**Fig. 8.** $10 \times 10$ $\mu$m$^2$ error signal AFM image of a SXCM imprint on a PMMA photo resist of a *Caenorhabditis elegans* nematode. A structural periodicity is clearly visible.

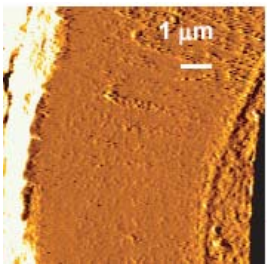


**Fig. 9.** $10 \times 10$ $\mu$m$^2$ error signal AFM image of a SXCM imprint on a PMMA photo resist of a *Caenorhabditis elegans* nematode. The image has been collected in the central region of nematode. A well characterized structure with a high roughness is visible near the nematode profile edge.

similar dimensions and are placed in the central region of the nematode profile. The dimension of the two structures, their position inside the worm, and the comparison with the nematode reconstruction (see Fig. 3) allow to identify them with the pharyngeal metacorpus and the terminal bulb of the nematode pharynx.

Several AFM images collected in the central region of SXCM imprint of *C. elegans* nematode show structures whose morphological characteristics allow to identify them as nuclei of different cell types. In particular, nuclei of three different cell types have been found. The comparison with Nomarsky microscopy data reported in literature [20] allowed to individuate and distinguish the round hypodermal and gut nuclei, having the characteristic "fried egg" appearance with a large and prominent nucleolus (Fig. 6a) and the smaller neuronal nuclei round and lacking in prominent nucleoli (Fig. 6b). Other type of cell nuclei has been imaged (Fig. 6c) but a clear correspondence to the data reported in literature has not been obtained.

A $10 \times 10$ $\mu$m$^2$ topography AFM image of the anterior body end of a *C. elegans* nematode is reported in Figure 7. The figure shows three small semicircular protrusions similar in shape to the characteristic six lips that symmetrically surround the buccal cavity of the *C. elegans* nematode. The side position of the *C. elegans* at the time of X-ray exposure is the reason why only three of the six lips are evidenced.

A doublet band pattern is visible in the $10 \times 10$ $\mu$m$^2$ error signal AFM image reported in Figure 8. This image reminds of the *C. elegans* cuticle organization. The picture shows regularly repeating bands giving rise to a structural periodicity ranging from 670 to 860 nm depending on the bending of the body worm. Even if Cox has reported a high variability in annulae width, nevertheless our in vivo results are slightly different from those obtained in sections of fixed and embedded specimens.

The image given in Figure 9 shows a well defined relief separating two areas having different roughness. This feature has been observed in many images collected in the nearly central region of different samples. On the basis of the recorded images and in the absence of further information from the experimental data it is not possible to give a definitive interpretation of these structures.

## 4 Conclusions

Results of SXCM investigation of *C. elegans* have been presented. It is the first time that SXCM has been applied to the study of multi-cellular biological organisms. Our results show that this technique may be a useful tool in biological research even with such complex samples. We would like to mention the possibility that, in our case, image formation may not be due to water window X-rays only. Indeed these may not be able to penetrate the nematode thickness ($\geq$10$-$30 $\mu$m). As a matter of fact, experimentally recorded X-ray spectra show the presence of X-rays at higher energy ($h\nu \geq 1$ keV). A large generation of hard X-rays is expected due to the fact that we used long laser wavelength, high laser intensities, and high $Z$ targets. Such hard X-rays can penetrate the sample more easily and give an important contribution to PMMA exposure and image formation. This could also explain the low contrast in many images (X-rays outside the water window are absorbed by water and proteins in almost similar way).

The goal of this work was to verify the potentiality of SXCM to investigate complex, multi-cellular biological samples. Thereby well characterized biological systems were used. In the present case well defined internal structures, cuticle features and organs have been imaged. In spite of many photo resists being analyzed, only a few showed identifiable structures. Probably, the nematode thickness and the consequent high X-ray absorption represent the mainly limiting factor. In fact, the AFM images showed a background profile in relief (height on PMMA 400 nm approximately), related to X-ray absorption by the whole nematode body, that could often hide its internal structures (which were characterized by a height on PMMA a few nm only on the background relief). In future experiments we need to improve the knowledge and control of many experimental parameters such as the water layer thickness, the X-ray beam intensity, the device geometry, the photo resist chemical development, as well as the sex of the biological samples and their embryonic development.

Authors thank the technical staffs of PALS for their overwhelming support in running the experiments. This work was performed under the E.U. contract HPRI-CT-1999-00053, Transnational Access to Major Research Infrastructures (ARI) of the Improving Human Potential (IHP) program of the 5th FP.

## References

1. H. Kondo, T. Tomie, J. Appl. Phys. **75**, 3798 (1994)
2. A.D. Stead, A.M. Page, T.W. Ford, Proc. SPIE **2523**, 40 (1995)
3. E. Turcu et al., Proc. SPIE **2015**, 243 (1994)
4. T.W. Ford, A.D. Stead, R.A. Cotton, Electron Microsc. Rev. **4**, 269 (1991)
5. J. Fletcher, R.A. Cotton, C. Webb, Proc. SPIE **1741**, 142 (1992)
6. G.F. Foster et al., Rev. Sci. Instrum. **63**, 599 (1992)
7. T.W. Ford et al., Proc. SPIE **1741**, 325 (1992)
8. A.D. Stead et al., Proc. SPIE **2523**, 202 (1995)
9. A. Masini et al., Proc. SPIE **3157**, 203 (1997)
10. D. Batani et al., Phys. Medica **14**, 151 (1998)
11. D. Batani et al., Phys. Medica **16**, 49 (2000)
12. K. Jungwirth et al., Phys. Plasmas **8**, 2495 (2001)
13. F. Bortolotto et al., Eur. Phys. J. D **11**, 309 (2000)
14. G.J. Tallents, JET Report No. JET-P(87), p. 56 (1987)
15. P.D. Rockett et al., Appl. Opt. **24**, 2536 (1985)
16. B.L. Henke, P.A. Jaanimag, Rev. Sci. Instrum. **56**, 1537 (1985)
17. B.L. Henke et al., J. Opt. Soc. Am. B **3**, 1540 (1986)
18. R.W. Lee, *User Manuel for RATION* (Lawrence Livermore National Laboratory, 1990)
19. G.N. Cox, S. Staprans, R.S. Edgar, Dev. Biol. **86**, 456 (1981)
20. C.I. Bargmann, L. Avery, Meth. Cell Biology **48**, 225 (1995)